Journal of Applied Physics

Low-energy electron impact dissociative recombination and vibrational transitions of N_2^+

Cite as: J. Appl. Phys. **129**, 053303 (2021); https://doi.org/10.1063/5.0038609
Submitted: 24 November 2020 . Accepted: 14 January 2021 . Published Online: 02 February 2021

A. Abdoulanziz, C. Argentin, V. Laporta, K. Chakrabarti, A. Bultel, J. Tennyson, I. F. Schneider, and J. Zs. Mezei

Journal of Applied Physics ARTICLE scitation.org/journal/jap

Low-energy electron impact dissociative recombination and vibrational transitions of N_2^+

Cite as: J. Appl. Phys. **129**, 053303 (2021); doi: 10.1063/5.0038609
Submitted: 24 November 2020 · Accepted: 14 January 2021 ·
Published Online: 2 February 2021

A. Abdoulanziz,[1] C. Argentin,[1,2] V. Laporta,[3] K. Chakrabarti,[4] A. Bultel,[2] J. Tennyson,[1,5] I. F. Schneider,[1,6,a)] and J. Zs. Mezei[1,7,b)]

AFFILIATIONS

[1]LOMC-UMR6294 CNRS-Université Le Havre Normandie, 76058 Le Havre, France
[2]CORIA-UMR6614 CNRS-Université de Rouen Normandie, 76800 Saint-Etienne du Rouvray, France
[3]Istituto per la Scienza e Tecnologia dei Plasmi, CNR, 70126 Bari, Italy
[4]Department of Mathematics, Scottish Church College, 700006 Kolkata, India
[5]Department of Physics and Astronomy, University College London, WC1E 6BT London, United Kingdom
[6]LAC-FRE2038, CNRS-Université Paris-Saclay, 91405 Orsay, France
[7]Institute for Nuclear Research, 4001 Debrecen, Hungary

Note: This paper is part of the Special Topic on Fundamentals and Applications of Atmospheric Pressure Plasmas.
[a)]**Electronic mail:** ioan.schneider@univ-lehavre.fr
[b)]**Author to whom correspondence should be addressed:** mezei.zsolt@atomki.hu

ABSTRACT

Cross sections and thermal rate coefficients are computed for electron-impact dissociative recombination and vibrational excitation/de-excitation of the N_2^+ molecular ion in its lowest six vibrational levels, for collision energies/temperatures up to 2.3 eV/5000 K.

I. INTRODUCTION

The nitrogen molecule N_2 is one of the most widely studied species so far in plasma physics. Being very stable at low temperature, it is very abundant in the Earth atmosphere and is notably present in other planetary atmospheres—Titan 98.4%,[1] Triton[2] Pluto,[3] Venus 3.5%, and Mars 1.9%.[1] For trans-Neptunian objects other than Pluto, this molecule is also one of the main components of the ices—spectroscopically observed at their surfaces—and may produce a very thin atmosphere when the temperature increases under solar irradiation.[4] Under the influence of an electric field, high altitude planetary atmosphere can be crossed by giant discharges of a few milliseconds duration called sprites, whose spectroscopic signature is mainly due to spontaneous emission from N_2 excited electronic states.[5] The application of N_2 as seeding gas in magnetically confined fusion plasmas (ITER and JET equipments) will help in the reduction of power loads on the tungsten divertor region. Nitrogen may be preferable as an extrinsic radiator to noble gases (neon) as it mostly affects the divertor radiation without significantly increasing core radiation.[6,7]

All these facts justify the various studies of the role of the N_2 molecule in the cold plasmas, from the state-to-state description of its electron impact induced reactivity[8–10] to the detailed modeling of its contribution to the plasma kinetics.[11–14]

Consequently, the N_2^+ cation is also of huge interest. Due to the solar irradiation, the production of N_2^+ on excited vibrational states plays a significant role in the characteristics of the Earth's thermosphere.[15] It is also the main molecular cation in the atmosphere of Titan[16] and Triton.[17] On the other hand, during the atmospheric entry of a spacecraft in Earth's and Titan's atmospheres, the hypersonic compression of the gases leads to the formation of a plasma departing from local thermodynamic equilibrium.[18] The ionic composition, including N_2^+, plays a key role in the radiation emitted by the plasma in the near UV spectral region.[19] In many plasma-assisted industrial processes elaborated so far, the plasma reactivity is greatly enhanced by the presence of N_2^+. This is, for instance, the case in the ammonia synthesis in plasmas/liquid processes.[20] N_2^+ is also very

effective in the antibacterial treatment of polyurethane surfaces.[21] Moreover, N_2^+—like N_2—is a key ingredient in the steel nitriding, resulting in improving its frictional wear resistance, surface hardness, and corrosion resistance.[22] Furthermore, N_2^+ also plays a major role in the dermatological treatments based on the nitrogen radio-frequency discharges.[23]

The characteristics of the nitrogen-containing plasmas cannot be fully understood without a deep knowledge of the reactivity of N_2^+, in particular, by collisions with electrons.

Dissociative Recombination (DR) is the major molecular cation destruction reaction that takes place when an electron collides with the N_2^+ molecular cation, leading to neutral atomic fragments,

$$N_2^+(v_i^+) + e^-(\varepsilon) \longrightarrow N + N. \quad (1)$$

Here, ε is the kinetic energy of the incident electron and v_i^+ is the initial vibrational quantum number of the target. Alongside DR, other competitive processes can occur,

$$N_2^+(v_i^+) + e^-(\varepsilon) \longrightarrow N_2^+(v_f^+) + e^-(\varepsilon_f), \quad (2)$$

i.e., elastic (EC) ($v_f^+ = v_i^+$), inelastic (IC) ($v_f^+ > v_i^+$) and super-elastic (SEC) collisions ($v_f^+ < v_i^+$), v_f^+ standing for the final vibrational quantum number of the target ion. These processes are also known as Elastic Scattering (ES), Vibrational Excitation (VE), and Vibrational deExcitation (VdE), respectively.

The elementary non-thermal electron driven processes, in particular, dissociative recombination, have been studied experimentally using plasmas with laser induced photo-fluorescence techniques,[24] shock tubes,[25] discharge afterglow experiments,[26,27] and microwave techniques.[28] The most detailed collisional data can be obtained in merged beam [29] and/or storage ring experiments.[30]

Two different sets of theoretical calculations have been performed[31–34] on the DR of N_2^+. They involved different underlying quantum chemistry but rather similar nuclear dynamics calculations; both these studies focused on the ground and the lowest three vibrational levels of the N_2^+ target.

While both results show good agreement with the experiment for the ground vibrational level, the rates for the higher vibrational levels calculated in Ref. 31, contrary to those of Refs. 32–34, indicate less strong vibrational dependence on temperature, in agreement with the experimental results.

Our aim with this paper is to extend as far as possible the calculations started in Ref. 31. This extension refers to

(i) The kinetic energy of the incoming electron: up to 2.3 eV vs 1 eV previously.
(ii) The elementary processes explored: besides the DR studied in the past, the VE and VdE cross sections and rate coefficients are computed.
(iii) The vibrational levels considered in the vibrational transitions: up to the fifth excited level of the target vs the third previously and the lowest ten vibrational levels as the final ones.

The rotational effects have been neglected since they are important only at very low collision energies.

All these extensions make our results relevant for the atmospheric and cold plasma environments, at electron temperatures where the rotational effects can be neglected.

The paper is organized as follows: After a brief description of the theoretical approach (Sec. II), we present in more detail the molecular data used in the calculations (Sec. III) followed by the presentation of the results (Sec. IV). The paper is ended with conclusions.

II. THEORETICAL APPROACH

The efficiency of our method of modeling the electron/diatomic cation collisions based on the Multichannel Quantum Defect Theory (MQDT) has been proved in many previous studies on different species, including H_2^+ and its isotopologues,[35–37] ArH^+,[38] CH^+,[39] SH^+,[40] etc. The general ideas of our approach were already presented in detail in our previous study of the N_2^+ dissociative recombination[31] and, therefore, here we restrict ourselves to its major steps.

The reactive processes (1) and (2) involve *ionization* channels—describing the scattering of an electron on the target cation - and *dissociation* channels—accounting for atom–atom scattering. The mixing of these channels results in quantum interference of the *direct* mechanism—in which the capture takes place into a doubly excited dissociative state of the neutral system—and the *indirect* one—in which the capture occurs via a Rydberg bound state of the molecule belonging to a *closed* channel, this state being predissociated by the dissociative one. In both mechanisms, the autoionization—based on the existence of *open* ionization channels—is

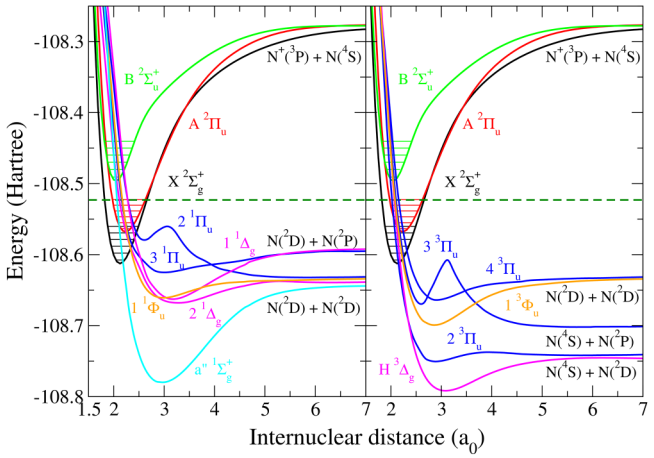

FIG. 1. Potential energy curves (PECs) relevant for the DR of N_2^+.[31] Target cation N_2^+: ground electronic state ($X^2\Sigma_g^+$) black, first excited state ($A^2\Pi_u$) red, and second excited state $B^2\Sigma_u^+$ green. Neutral system N_2: Left panel, singlet states of different symmetries—blue for $^1\Pi_u$, magenta for $^1\Delta_g$, cyan for $a''^1\Sigma_g^+$, and orange for $^1\Phi_u$. Right panel, triplet states of different symmetries—blue for $^3\Pi_u$, magenta for $H^3\Delta_g$, and orange for $^3\Phi_u$. The lowest five vibrational levels of each electronic state of the ion and the dissociative asymptotic limits for all states are shown. The green dashed line gives the upper limit of the total energy of the system, above which our results are still reasonably correct (see the text).

in competition with the predissociation and can lead to the excitation or to the de-excitation of the cation.

One starts with the building of the *interaction matrix* $\mathscr{V}$ that drives the collision, whose elements quantify the couplings between the different channels—ionization and/or dissociation ones.

More specifically, each of the ionization channels, built on the N_2^+ ion in one of its three lowest electronic states—$X\ ^2\Sigma_g^+$, $A\ ^2\Pi_u$, or $B\ ^2\Sigma_u^+$, see Fig. 1—in a particular vibrational level, interacts not only with all the dissociation exit channels (Rydberg–valence interaction), but also with the other ionization channels (Rydberg–Rydberg interactions)—Fig. 2. Depending on the total energy of the system, these ionization channels can be *open*—either as entrance channels, describing the incident electron colliding the ion in its ground electronic state, or as exit channels, describing the autoionization, i.e., elastic scattering, vibrational excitation, and de-excitation—or *closed*—describing the resonant temporary captures into Rydberg states.

Once the $\mathscr{V}$-matrix is elaborated, we build the short-range reaction matrix $\mathscr{K}$ of the collision, as a second order perturbative solution of the Lippmann–Schwinger equation. The diagonalized version of the $\mathscr{K}$-matrix (in the eigenchannel representation), whose eigenvalues are expressed in terms of long range phase-shifts of the eigenfunctions, together with the vibronic couplings between the ionization channels, serves for the building of the frame transformation matrices.

Applying a Cayley transformation on these latter matrices, we can setup the generalized scattering matrix X. The Seaton's method of "eliminating" the closed channels[41] is then employed, resulting in the physical scattering matrix $\mathscr{S}$,

$$\boldsymbol{S} = \boldsymbol{X}_{oo} - \boldsymbol{X}_{oc}\frac{1}{\boldsymbol{X}_{cc} - \exp(-\mathrm{i}\ 2\ \pi\boldsymbol{\nu})}\boldsymbol{X}_{co}, \tag{3}$$

relying on the block-matrices involving open (X_{oo}), open and closed (X_{oc} and X_{co}), and closed (X_{cc}) channels. The diagonal matrix ν in the denominator of Eq. (3) contains the effective quantum numbers corresponding to the vibrational thresholds of the closed ionization channels at a given total energy of the system.

Finally, the cross section for the dissociative recombination and for the vibrational transitions—vibrational excitation/de-excitation and elastic scattering write, respectively, as

$$\sigma_{diss\leftarrow v_i^+} = \frac{\pi}{4\varepsilon}\rho^{sym}\sum_{l,j}\left|S^{\Lambda}_{d_j,lv_i^+}\right|^2 \tag{4}$$

and

$$\sigma_{v_f^+\leftarrow v_i^+} = \frac{\pi}{4\varepsilon}\rho^{sym}\sum_{l,l'}\left|S^{\Lambda}_{l'v_f^+,lv_i^+} - \delta_{l,l'}\delta_{v_i^+,v_f^+}\right|^2, \tag{5}$$

where d_j stands for a given dissociative state and ρ^{sym} the ratio between the state multiplicities of the neutral and the target ion.

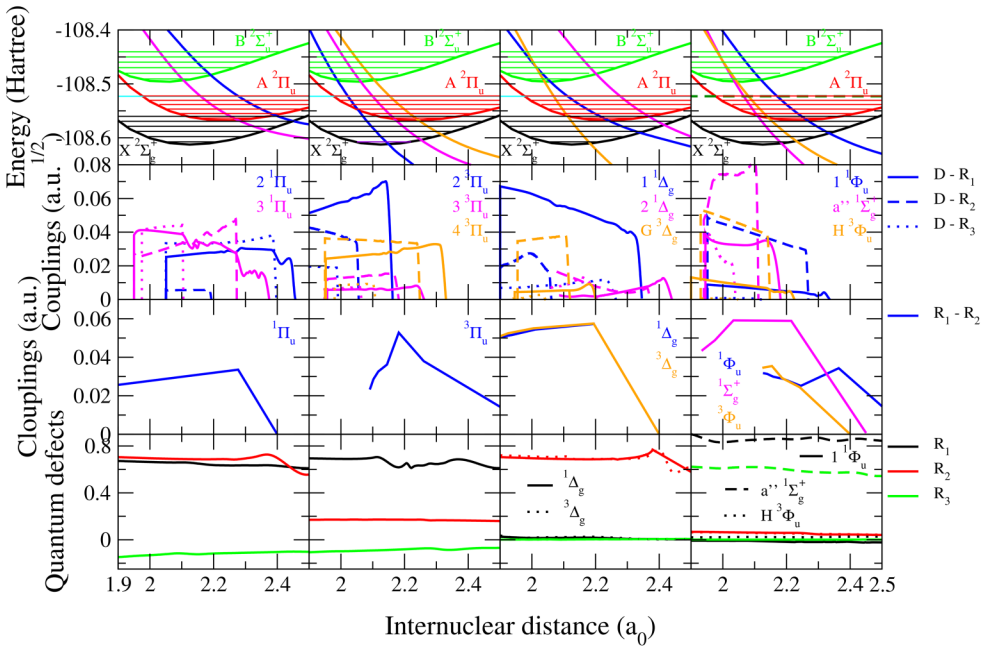

FIG. 2. Molecular data sets for the modeling of reactive collisions between electrons and N_2^+.[31] First row: PECs of the relevant states of the ion and of the neutral for all relevant symmetries. Second row: Rydberg–valence electronic couplings. Third row: Rydberg–Rydberg electronic couplings. Fourth row: Quantum defects characterizing the Rydberg series of states.

TABLE I. The energies of the vibrational levels of the N_2^+ molecular cation—relative to the ground one—involved either as initial or as final levels in the present calculations.

v^+	0	1	2	3	4	5	6	7	8	9
E_{v^+} (eV)	0.0	0.266	0.528	0.786	1.040	1.290	1.536	1.777	2.014	2.248

III. MOLECULAR DATA

The nuclear dynamics in low-energy electron/molecular cation collisions crucially depends on the molecular structure of the target and of the formed neutral—often superexcited—complex. The relevant molecular data sets consist in the potential energy curves (PECs) of the target cation—for the ground and for the excited electronic states—the PECs of the doubly excited bound or dissociative molecular states of the neutral, the quantum defect-functions characterizing the bound mono-excited Rydberg series of the neutral, and the coupling functions between the several—ionization and dissociation—continua.

One of the few quantum chemistry methods capable of producing the highly excited molecular states at the required accuracy is based on the R-Matrix Theory.[42] Bound and resonant adiabatic potential energy curves of the valence and Rydberg states of N_2 having singlet and triplet symmetries were obtained by Little and Tennyson[43,44] using R-matrix calculations on fine grid of internuclear separations. The diabatic curves, couplings, and quantum defects relevant for the dissociative recombination of N_2^+ were presented in Ref. 31. The electronic states of the target were calculated using the standard quantum chemistry program suite Molpro.[45] Figure 1 shows the PECs of the dissociative molecular states of N_2, as well as those of the relevant states of N_2^+, involved in our previous[31] and present calculations.

The same PECs are displayed by symmetries on the first row of Fig. 2, which contains the whole ensemble of molecular data relevant for the modeling of the internuclear dynamics. Whereas its first row illustrates how favorable the crossings are between the PECs of the dissociative states with those of the target ones—i.e., the Franck–Condon effect—the driving interactions of the dynamics—the Rydberg–valence couplings—are shown in the second row. The third row gives the Rydberg–Rydberg couplings: In the present calculation, only the couplings among the series correlating to the ground (X) and first excited (A) state of the ion have been considered. And finally, the last row of the figure displays the quantum defects characterizing the Rydberg series built, each of them, on one of the three cores X, A, and B.

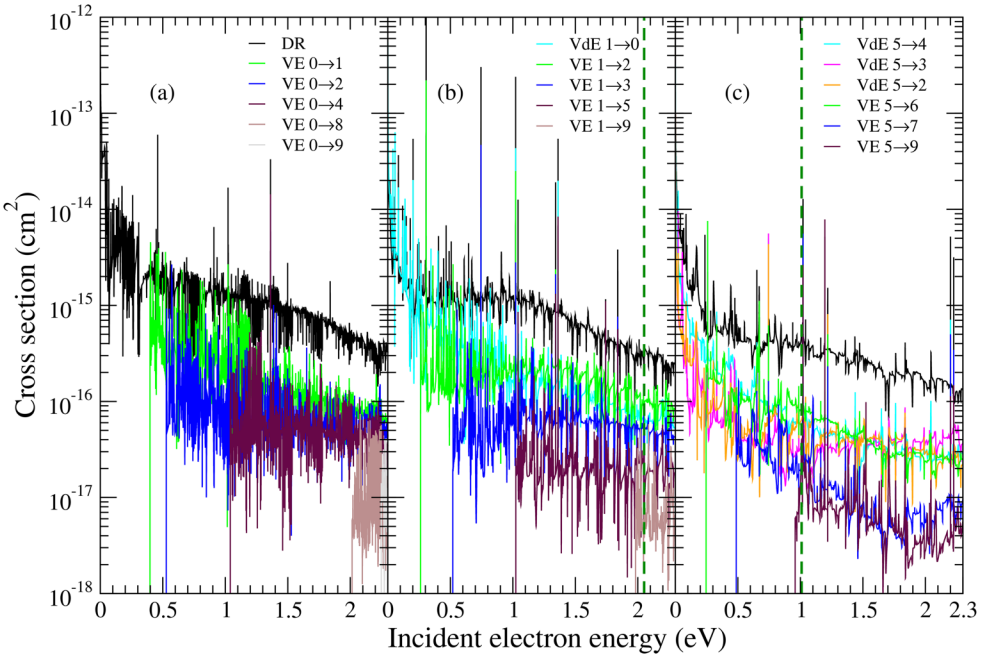

FIG. 3. Global DR, VE, and VdE cross sections of the N_2^+ $v_i^+ = 0$ (a), $v_i^+ = 1$ (b), and $v_i^+ = 5$ (c) as a function of the collision energy. For vibrational transitions (VE and VdE), we label the processes as transitions from the initial to the final vibrational levels of the target. The vertical dashed dark-green line gives the precision limit of the calculations (for details, see the text).

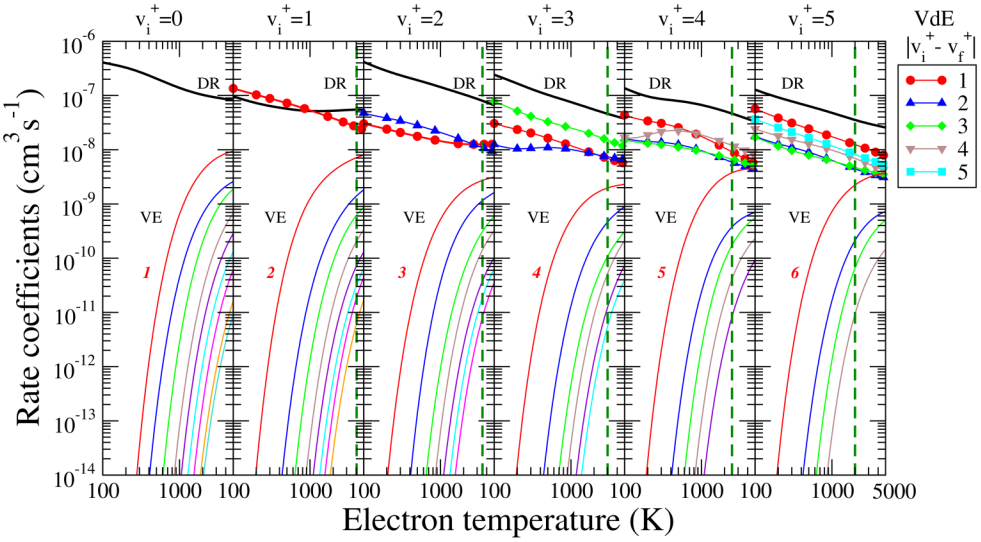

FIG. 4. Maxwell rate coefficients for all the relevant electron-induced processes on N_2^+ initially on $v_i^+ = 0$–5 vibrational levels: Dissociative recombination (black line), vibrational excitation (thin colored lines), and vibrational de-excitation (symbols and thick colored lines). For the vibrational excitations, all the transitions are shown up to $v_f^+ = 9$ with the lowest transition being labeled on each figure. The excitation and the de-excitation up to the final vibrational quantum numbers are given. The green dashed line gives the precision limit of our calculation given in temperatures (for details, see the text).

IV. RESULTS AND DISCUSSIONS

Based on the molecular data already presented in Fig. 2, we have performed nuclear dynamics calculations using the MQDT approach presented in Sec. II. The DR, VE, and VdE cross sections have been calculated considering the N_2^+ target in one of its lowest six vibrational states and focusing on the vibrational transitions to the lowest ten vibrational levels, when energetically accessible. Table I shows the energies of these latter levels relative to $v_i^+ = 0$ of the target.

The calculations have been performed by taking into account both the *direct* and the *indirect* mechanisms, the reaction matrix being evaluated in the second order, and all their vibrational levels—81, 66, and 50, respectively, associated with *open* or *closed* ionization channels, according to the total energy of the system—have been fully accounted for.

The cross sections have been calculated for all the relevant symmetries listed in Figs. 1 and 2, for collision energies of the incident electron ranging between 10^{-5} and 2.3 eV, with an energy step of 0.01 meV. These cross sections have been summed up to obtain the global cross sections.

The global DR, VE, and VdE cross sections for target cations having initial vibrational levels $v_i^+ = 0$, 1, and 5 are shown in Figs. 3(a)–3(c), respectively. The vertical dark-green dashed lines in the mid and upper panels of Fig. 3 mark the energy below which the calculations are the most accurate. Above these thresholds, the calculations neglect the role of the higher lying dissociative states of the neutral.

TABLE II. List of the fitting parameters used in formula (6), temperature regions, and root mean squares for the DR rate coefficients of N_2^+ ($v_i^+ = 0$–5).

	v_i^+	Temperature range K	A ($cm^3\ s^{-1}\ K^{-\alpha}$)	α	B (K)	RMS
DR	0	100≤T≤700	$1.560\,20\times10^{-5}$	−0.679 449	53.0333	0.0051
		700<T≤5000	$2.270\,99\times10^{-7}$	−0.129 049	−388.399	0.0040
	1	100≤T≤900	$1.111\,78\times10^{-7}$	−0.120 373	−41.6843	0.0049
		900<T≤5000	$2.607\,04\times10^{-8}$	0.086 645	−85.4307	0.0055
	2	100≤T≤1000	$1.544\,30\times10^{-6}$	−0.345 836	−28.1712	0.0053
		1000<T≤5000	$7.095\,92\times10^{-6}$	−0.544 674	145.630	0.0030
	3	100≤T≤5000	$1.530\,33\times10^{-6}$	−0.438 705	−19.1368	0.0088
	4	100≤T≤460	$5.255\,73\times10^{-8}$	0.0423 84	−76.5345	0.0032
		460<T≤5000	$3.426\,00\times10^{-6}$	−0.539 469	208.028	0.0031
	5	100≤T≤5000	$7.206\,27\times10^{-7}$	−0.394 354	−7.90548	0.0106

TABLE III. List of the fitting parameters used in formula (6), temperature regions and root mean squares for the VE and VdE rate coefficients of N_2^+ ($v_i^+ = 0 - 5$ and $v_i^+ = 9$). The lines having bold v_f^+ values belong to VdE.

v_i^+	v_f^+	Temperature range (K)	A ($cm^3 s^{-1} K^{-\alpha}$)	α	B (K)	RMS
0	1	270≤T≤5000	$3.354\,76\times10^{-6}$	−0.584 062	4525.43	0.0073
	2	400≤T≤1000	$9.136\,78\times10^{-7}$	−0.553 899	6100.88	0.0021
		1000<T≤5000	$3.045\,96\times10^{-7}$	−0.420 925	5907.02	0.0028
	3	600≤T≤1500	$9.670\,70\times10^{-7}$	−0.509 170	3228.55	0.0062
		1500<T≤5000	$4.984\,32\times10^{-6}$	−0.699 380	9626.89	0.0040
	4	850≤T≤2000	$9.306\,28\times10^{-8}$	−0.292 379	119 89.3	0.0054
		2000<T≤5000	$8.814\,69\times10^{-7}$	−0.546 342	126 51.0	0.0033
	5	1000≤T≤5000	$8.924\,93\times10^{-7}$	−0.596 125	14871.8	0.0066
	6	1200≤T≤2500	$1.447\,02\times10^{-6}$	−0.667 566	179 80.5	0.0022
		2500<T≤5000	$5.491\,26\times10^{-6}$	−0.815 886	184 22.2	0.0009
	7	1500≤T≤5000	$1.655\,52\times10^{-6}$	−0.696 318	213 45.0	0.0190
	8	1800≤T≤5000	$9.867\,09\times10^{-8}$	−0.470 871	235 04.3	0.0071
	9	2000≤T≤5000	$1.340\,02\times10^{-6}$	−0.780 327	263 09.7	0.0025
1	**0**	100≤T≤5000	$1.453\,41\times10^{-6}$	−0.478 820	19.3876	0.0195
	2	190≤T≤900	$3.828\,42\times10^{-6}$	−0.706 740	3146.96	0.0154
		900<T≤5000	$1.451\,26\times10^{-8}$	−0.015 912	2326.31	0.0076
	3	420≤T≤900	$1.790\,64\times10^{-7}$	−0.420 497	6137.15	0.0011
		900<T≤5000	$1.143\,29\times10^{-8}$	−0.080 877	5736.89	0.0040
	4	600≤T≤1500	$5.536\,86\times10^{-8}$	−0.277 018	8726.55	0.0040
		1500<T≤5000	$4.120\,85\times10^{-7}$	−0.506 359	9262.99	0.0065
	5	850≤T≤5000	$1.382\,79\times10^{-7}$	−0.426 255	120 08.4	0.0031
	6	1100≤T≤2500	$9.873\,96\times10^{-7}$	−0.707 100	148 13.1	0.0035
		2500<T≤5000	$3.024\,02\times10^{-8}$	−0.318 434	136 84.3	0.0017
	7	1300≤T≤5000	$3.250\,83\times10^{-8}$	−0.336 661	167 32.0	0.0157
	8	1500≤T≤5000	$1.395\,45\times10^{-7}$	−0.467 278	203 48.3	0.0062
	9	1800≤T≤5000	$3.505\,37\times10^{-8}$	−0.362 041	226 92.0	0.0027
2	**1**	100≤T≤1500	$1.046\,03\times10^{-7}$	−0.287 973	−9.07849	0.0073
		1500<T≤5000	$4.350\,37\times10^{-9}$	0.116 715	−377.074	0.0027
	0	100≤T≤5000	$6.634\,40\times10^{-7}$	−0.498 417	38.4238	0.0193
	3	200≤T≤700	$1.791\,99\times10^{-7}$	−0.415 799	2977.42	0.0005
		700<T≤5000	$7.478\,37\times10^{-8}$	−0.306 566	2843.67	0.0089
	4	400≤T≤1300	$4.275\,98\times10^{-6}$	−0.800 392	6144.90	0.0036
		1300<T≤5000	$4.375\,39\times10^{-8}$	−0.268 995	5056.36	0.0148
	5	600≤T≤1500	$7.029\,48\times10^{-8}$	−0.367 691	8687.59	0.0076
		1500<T≤5000	$8.342\,12\times10^{-9}$	−0.117 668	8217.86	0.0022
	6	850≤T≤5000	$9.678\,64\times10^{-8}$	−0.401 678	114 29.0	0.0164
	7	1000≤T≤2500	$9.385\,61\times10^{-7}$	−0.733 592	145 27.8	0.0013
		2500<T≤5000	$1.752\,59\times10^{-7}$	−0.547 538	139 60.8	0.0012
	8	1300≤T≤5000	$1.130\,24\times10^{-6}$	−0.737 221	175 18.6	0.0117
	9	1500≤T≤5000	$1.462\,92\times10^{-7}$	−0.513 870	197 32.3	0.0137
3	**2**	100≤T≤5000	$3.601\,61\times10^{-7}$	−0.490 909	23.3038	0.0108
	1	100≤T<700	$2.526\,73\times10^{-9}$	0.215 750	−58.7472	0.0174
		700≤T<5000	$7.862\,65\times10^{-8}$	−0.292 543	41.8077	0.0060
	0	100≤T≤700	3.69265×10^{-7}	−0.399 263	−29.4462	0.0087
		700<T≤5000	$1.889\,55\times10^{-6}$	−0.594 995	205.425	0.0045
	4	100≤T≤560	$3.679\,69\times10^{-7}$	−0.546 948	2807.96	0.0290
		560<T≤5000	$1.291\,98\times10^{-7}$	−0.410 534	2682.71	0.0112
	5	440≤T≤1300	$4.829\,97\times10^{-7}$	−0.335 457	5887.42	0.0106
		1300<T≤5000	$8.499\,83\times10^{-9}$	−0.137 448	5427.34	0.0084
	6	650≤T≤1700	$1.541\,45\times10^{-7}$	−0.532 191	9039.15	0.0032
		1300<T≤5000	$9.065\,25\times10^{-10}$	0.052 019	7617.98	0.0111
	7	850≤T≤2000	$2.496\,01\times10^{-8}$	−0.300 658	113 33.8	0.0091

TABLE III. (*Continued.*)

v_i^+	v_f^+	Temperature range (K)	A ($cm^3s^{-1}K^{-\alpha}$)	α	B (K)	RMS
		2000<T≤5000	$4.154\,24\times10^{-9}$	−0.093 853	108 88.7	0.0003
	8	1100≤T≤5000	$2.275\,58\times10^{-9}$	−0.079 760	137 23.8	0.0189
	9	1300≤T≤5000	$3.068\,56\times10^{-7}$	−0.645 208	172 78.8	0.0034
4	**3**	100≤T≤400	$6.378\,63\times10^{-8}$	−0.145 968	−28.4720	0.0082
		400<T≤5000	$6.361\,81\times10^{-6}$	−0.825 697	192.216	0.0072
	2	100≤T≤900	$6.554\,02\times10^{-8}$	−0.262 797	23.6274	0.0227
		900<T≤5000	$1.058\,21\times10^{-7}$	−0.378 427	−214.371	0.0140
	1	100≤T≤440	$2.329\,72\times10^{-8}$	−0.116 666	−8.972 62	0.0057
		440≤T≤5000	$2.270\,97\times10^{-7}$	−0.444 141	124.096	0.0044
	0	100≤T≤400	$2.129\,11\times10^{-9}$	0.389 295	−22.4417	0.0183
		400<T≤5000	$2.100\,16\times10^{-6}$	−0.645 580	264.431	0.0066
	5	190≤T≤900	$7.698\,58\times10^{-7}$	−0.525 187	2964.92	0.0217
		900<T≤5000	$2.432\,98\times10^{-6}$	−0.666 480	3146.71	0.0028
	6	400≤T≤1200	$4.497\,41\times10^{-6}$	−0.896 475	5955.41	0.0017
		1200<T≤5000	$8.844\,87\times10^{-7}$	−0.708 372	5563.92	0.0076
	7	580≤T≤1500	$1.179\,91\times10^{-5}$	−0.974 002	8780.06	0.0036
		1500<T≤5000	$7.346\,77\times10^{-7}$	−0.655 786	8053.50	0.0084
	8	800≤T≤2000	$4.107\,91\times10^{-6}$	−0.886 512	11 434.1	0.0015
		2000<T≤5000	$3.732\,24\times10^{-7}$	−0.615 368	107 37.3	0.0026
	9	1000≤T≤2500	$1.137\,54\times10^{-7}$	−0.519 202	136 77.4	0.0126
		2500<T≤5000	$1.251\,00\times10^{-8}$	−0.269 595	130 39.9	0.0002
5	**4**	100≤T≤5000	$4.509\,70\times10^{-7}$	−0.474 388	−11.0566	0.0125
	3	100≤T≤500	$5.830\,98\times10^{-8}$	−0.304 037	−19.8859	0.0073
		500<T≤5000	$1.317\,81\times10^{-7}$	−0.447 966	−55.6242	0.0132
	2	100≤T≤5000	$6.216\,86\times10^{-8}$	−0.340 696	−27.4858	0.0101
	1	100≤T≤900	$8.495\,09\times10^{-8}$	−0.310 555	−17.4355	0.0022
		900<T≤5000	$1.089\,34\times10^{-6}$	−0.653 000	198.309	0.0031
	0	100≤T≤5000	$3.732\,56\times10^{-7}$	−0.501 538	2.803 63	0.0122
	6	190≤T≤5000	$1.476\,02\times10^{-7}$	−0.367 489	2789.39	0.0150
	7	400≤T≤1200	$3.158\,77\times10^{-8}$	−0.292 229	5543.78	0.0036
		1200<T≤5000	$1.105\,25\times10^{-6}$	−0.712 115	6289.63	0.0090
	8	600≤T≤5000	$4.107\,24\times10^{-7}$	−0.585 006	8593.14	0.0153
	9	850≤T≤2000	$7.616\,66\times10^{-7}$	−0.744 946	113 07.6	0.0038
		2000<T≤5000	$7.878\,95\times10^{-8}$	−0.489 941	106 18.0	0.0036

Nevertheless, the data displayed continue to be reasonably correct above these thresholds because these dissociative states penetrate into the ionization continuum well above these thresholds, forming favorable/non-vanishing Franck–Condon overlaps with the target electronic states at even higher collision energies. This Franck–Condon overlap is proportional to the first order term of the direct cross section. In addition, the couplings of these dissociative states with the Rydberg series are generally weaker, leading to less important cross sections in second order.

The *direct* mechanism is responsible for the background $1/E$ behavior of the cross sections, while the *indirect* one through the temporary capture into the Rydberg states produces all the resonance structures dominating the cross sections.

Among all the processes studied here, dissociative recombination (black curves in Fig. 3) predominates. The global DR cross section increases as we change the initial vibrational state of the target by unity and starts to decrease as we arrive at $v_i^+ = 5$. While the vibrational de-excitation (cyan curves for initial vibrational levels higher than 0) is in competition with the DR cross section, at higher collision energies their overall cross section values are at least with a factor of 5 smaller than those of the DR. The vibrational excitations (green, blue, violet, maroon, etc., curves) show threshold effects at the collision energies where they become open. Moreover, one can see that for a given initial vibrational level v_i^+ the $|\Delta v^+| = 1$ vibrational transitions are the most probable ones, decreasing monotonically with $|\Delta v^+|$ for the transitions between more distant levels.

Figure 4 shows the thermal rate coefficients of all processes for the six lowest initial vibrational levels of N_2^+. The green dashed line gives the precision limits of our calculation expressed now in electron temperatures.

The DR (solid black line in Fig. 4) and VdE (symbols and thick colored lines) rate coefficients decrease monotonically with the temperature, while the VE (thin colored lines) ones increase, partly because of the threshold behavior of their corresponding

cross sections. The largest rate coefficients we obtained are those for the DR. With the exception of the $v_i^+ = 1$ case, the VdE rate coefficients are smaller than those for the DR. At $v_i^+ = 1$, the DR is in competition with VdE but, for $v_i^+ > 1$, DR exceeds VdE by a factor of 2–5. We can see from Fig. 4 that the VE process is relatively important at high electron temperatures only. Moreover, the higher we go with the initial vibrational quantum number of the target cation, the more probable VE becomes.

And finally, in order to allow the versatile implementation of the rate coefficients in kinetics modeling codes, we have fitted them with Arrhenius-type formulas. The calculated rate coefficients for the dissociative recombination of electrons with N_2^+ in each of its lowest 6 vibrational levels ($v_i^+ = 0, 1, \ldots, 5$) have been interpolated using the mathematical form,

$$k^{fitt}(T) = A\, T^{\alpha}\, \exp\left[-\frac{B}{T}\right] \tag{6}$$

over the electron temperature range $100\ \mathrm{K} \leq T_e \leq 5\ 000\ \mathrm{K}$ and/or for rate coefficients larger than 10^{-14} $\mathrm{cm^3\ s^{-1}}$, as displayed in Fig. 4. The A, α, and B fitting parameters used in Eq. (6) together with the temperature regions are listed in Table II for DR and in Table III for VE and VdE processes. The efficiency of the fitting is characterized by the root mean squares, and we were able to reproduce the MQDT rate coefficients with a precision higher than 97%.

V. CONCLUSIONS

The present work extends considerably our previous study of the dissociative recombination of N_2^+ with electrons.[31] Making use of the molecular data set calculated in Refs. 31, 43, and 44 and of our stepwise MQDT method, we have performed calculations for the lowest 6 vibrational levels of the target cation in collision with electrons having kinetic energy up 2.3 eV and, in the case of thermal equilibrium, electronic temperature up to 5000 K. We have provided cross sections and rate coefficients for dissociative recombination, vibrational excitation, and de-excitation of the N_2^+ molecular cation, important for the detailed kinetic modeling of cold astrophysical, atmospheric, and laboratory plasmas. The calculated cross sections and rate coefficients are available on request.

ACKNOWLEDGMENTS

The authors acknowledge support from Fédération de Recherche Fusion par Confinement Magnétique (CNRS and CEA), La Région Normandie, FEDER, and LabEx EMC3 via the projects PTOLEMEE, Bioengine, EMoPlaF, COMUE Normandie Université, the Institute for Energy, Propulsion and Environment (FR-IEPE), the European Union via COST (European Cooperation in Science and Technology) action MD-GAS (CA18212), and ERASMUS-plus conventions between Université Le Havre Normandie and University College London. This work has received funding from the Euratom Research and Training Programme 2014–2018 and 2019–2020 under Grant Agreement No. 633053. The views and opinions expressed herein do not necessarily reflect those of the European Commission. The authors are indebted to Agence Nationale de la Recherche (ANR) via the project MONA, Centre National de la Recherche Scientifique via the GdR TheMS and the DYMCOM project, and the Institute Pascal, University Paris-Saclay for the warm hospitality during the DYMCOM workshop. This work was supported by the Programme National "Physique et Chimie du Milieu Interstellaire" (PCMI) of CNRS/INSU with INC/INP co-funded by CEA and CNES. J.Zs.M. thanks the financial support of the National Research, Development and Innovation Fund of Hungary, under the K18 funding scheme with Project No. K128621.

DATA AVAILABILITY

The data that support the findings of this study are available from the corresponding author upon reasonable request.

REFERENCES

[1]V. A. Krasnopolsky, "Chemical composition of Titan's atmosphere and ionosphere: Observations and the photochemical model," Icarus **236**, 83–91 (2014).
[2]J. L. Elliot, D. F. Strobel, X. Zhu, J. A. Stansberry, L. H. Wasserman, and O. G. Franz, "The thermal structure of Triton's middle atmosphere," Icarus **143**, 425–428 (2020).
[3]V. A. Krasnopolsky, "A photochemical model of Pluto's atmosphere and ionosphere," Icarus **335**, 113374 (2020).
[4]L. A. Young, F. Braga-Ribas, and R. E. Johnson, "Volatile evolution and atmospheres of trans-neptunian objects," in *The Trans-Neptunian Solar System*, edited by D. Prialnik, M. A. Barucci, and L. A. Young (Elsevier, The Netherlands, 2020), Chap. 6, pp. 127–151.
[5]R. A. Armstrong, D. M. Suszcynsky, W. A. Lyons, and T. E. Nelson, "Multi-color photometric measurements of ionization and energies in sprites," Geophys. Res. Lett. **27**, 653–656 (2000).
[6]M. Oberkofler *et al.*, "First nitrogen-seeding experiments in jet with the ITER-like wall," J. Nucl. Mater. **438**, S258 (2013).
[7]C. Giroud and JET-EFDA Contributors *et al.*, "(Exc/p3-02) integration of a radiative divertor for heat load control into jet operational scenarios," in *Proceedings of the 23rd IAEA Fusion Energy Conference, Daejeon, 11–16 October 2010* (International Atomic Energy Agency, 2010).
[8]V. Laporta, R. Celiberto, and J. M. Wadehra, "Theoretical vibrational-excitation cross sections and rate coefficients for electron-impact resonant collisions involving rovibrationally excited N_2 and NO molecules," Plasma Sources Sci. Technol. **21**, 055018 (2012).
[9]V. Laporta, D. A. Little, R. Celiberto, and J. Tennyson, "Electron-impact resonant vibrational excitation and dissociation processes involving vibrationally excited N_2 molecules," Plasma Sources Sci. Technol. **23**, 065002 (2014).
[10]M. Kitajima, T. Kishino, T. Okumura, N. Kobayashi, A. Sayama, Y. Mori, K. Hosaka, T. Odagiri, M. Hoshino, and H. Tanaka, "Low-energy and very-low energy total cross sections for electron collisions with N_2," Eur. Phys. J. D **71**, 139 (2017).
[11]V. Guerra, P. A. Sa, and J. Loureiro, "Kinetic modeling of low-pressure nitrogen discharges and post-discharges," Eur. Phys. J. Appl. Phys. **28**, 125 (2004).
[12]M. Panesi, T. E. Magin, A. Bourdon, A. Bultel, and O. Chazot, "Electronic excitation of atoms and molecules for the FIRE II flight experiment," J. Thermophys. Heat Trans. **25**, 361 (2011).
[13]M. Capitelli, G. Colonna, G. D'Ammando, V. Laporta, and A. Laricchiuta, "Nonequilibrium dissociation mechanisms in low temperature nitrogen and carbon monoxide plasmas," Chem. Phys. **438**, 31 (2014).
[14]K. L. Heritier, R. L. Jaffe, V. Laporta, and M. Panesi, "Energy transfer models in nitrogen plasmas: Analysis of $N_2(x^1\sigma_g^+)$–$n(^4s_u) - e^-$ interaction," J. Chem. Phys. **141**, 184302 (2014).
[15]M. R. Torr, "Neutral and ioan chemistry and solar fluxes," J. Geomag. Geoelectr. **35**, 131–153 (1983).
[16]H. Lammer, W. Stumptner, G. Molina-Cuberos, S. Bauer, and T. Owen, "Nitrogen isotope fractionation and its consequence for Titan's atmospheric evolution," Planet. Space Sci. **48**, 529–543 (2000).

[17]Y. L. Yung and J. R. Lyons, "Triton: Topside ionosphere and nitrogen escape," Geophys. Res. Lett. **17**, 1717–1720 (1990).
[18]J. Annaloro and A. Bultel, "Vibrational and electronic collisional-radiative model in air for earth entry problems," Phys. Plasmas **21**, 123512 (2020).
[19]Y. Plastinin, G. Karabadzhak, B. Khmelinin, B. Zemliansky, A. Gorshkov, and G. Zalogin, "Measurements of the UV radiation generated by the Soyuz spacecraft transport capsule during reentry," in *45th AIAA Aerospace Sciences Meeting and Exhibit* (AIAA, 2007/2012), https://arc.aiaa.org/doi/pdf/10.2514/6.2007-815.
[20]T. Sakakura, N. Murakami, Y. Takatsuji, M. Morimoto, and T. Haruyama, "Contribution of discharge excited atomic N, N_2^*, and N_2^+ to a plasma/liquid interfacial reaction as suggested by quantitative analysis," Chem. Phys. Chem. **20**, 1467–1474 (2019).
[21]I. A. Morozov, A. S. Mamaev, I. V. Osorgina, L. M. Lemkina, V. P. Korobov, A. Y. Belyaev, S. E. Porozova, and M. G. Sherban, "Structural-mechanical and antibacterial properties of a soft elastic polyurethane surface after plasma immersion N_2^+ implantation," Mater. Sci. Eng. C **62**, 242–248 (2016).
[22]M. K. Sharma and B. K. Saikia, "Discharge conditions and emission spectroscopy of N_2 and N_2^+ active species in a variable power DC pulsed plasma used for steel nitriding," Indian J. Pure Appl. Phys. **46**, 463–470 (2008); available at http://nopr.niscair.res.in/handle/123456789/1889.
[23]J. D. Holcomb and A. Schucker, "Helium plasma skin regeneration: Evaluation of skin tissue effects in a porcine model and comparison to nitrogen plasma skin regeneration," Lasers Surg. Med. **52**, 23–32 (2020).
[24]E. C. Zipf, "The dissociative recombination of vibrationally excited N_2^+ ions," Geophys. Res. Lett. **7**, 645–648 (1980).
[25]A. J. Cunningham and R. M. Hobson, "Dissociative recombination at elevated temperatures. IV. N_2^+ dominated afterglows," J. Phys. B At. Mol. Phys. **5**, 2328–2331 (1972).
[26]S. K. Mitra, "Active nitrogen," Phys. Rev. **90**, 516–521 (1953).
[27]J. Kaplan, "Active nitrogen," Phys. Rev. **73**, 494–496 (1948).
[28]M. A. Biondi and S. C. Brown, "Measurement of electron-ion recombination," Phys. Rev. **76**, 1697–1700 (1949).
[29]C. Noren, F. B. Yousif, and J. B. A. Mitchell, "Dissociative recombination and excitation of N_2^+," J. Chem. Soc. Faraday Trans. 2 **85**, 1697 (1989).
[30]J. R. Peterson, A. L. Padellec, H. Danared, G. H. Dunn, M. Larsson, A. Larson, R. Peverall, C. Strömholm, S. Rosén, M. af Ugglas, and W. J. van der Zande, "Dissociative recombination and excitation of N_2^+: Cross sections and product branching ratios," J. Chem. Phys. **108**, 1978–1988 (1998).
[31]D. A. Little, K. Chakrabarti, J. Z. Mezei, I. F. Schneider, and J. Tennyson, "Dissociative recombination of N+2 : An ab initio study," Phys. Rev. A **90**, 052705 (2014).
[32]S. L. Guberman, "Spectroscopy above the ionization threshold: Dissociative recombination of the ground vibrational level of N_2^+," J. Chem. Phys. **137**, 074309 (2012).
[33]S. L. Guberman, "The vibrational dependence of dissociative recombination: Cross sections for N_2^+," J. Chem. Phys. **139**, 124318 (2013).
[34]S. L. Guberman, "The vibrational dependence of dissociative recombination: Rate constants for N_2^+," J. Chem. Phys. **141**, 204307 (2014).
[35]K. Chakrabarti, D. R. Backodissa-Kiminou, N. Pop, J. Z. Mezei, O. Motapon, F. Lique, O. Dulieu, A. Wolf, and I. F. Schneider, "Dissociative recombination of electrons with diatomic molecular cations above dissociation threshold: Application to H_2+ and HD+," Phys. Rev. A **87**, 022702 (2013).
[36]O. Motapon, N. Pop, F. Argoubi, J. Z. Mezei, M. D. Epee Epee, A. Faure, M. Telmini, J. Tennyson, and I. F. Schneider, "Rotational transitions induced by collisions of HD^+ ions with low-energy electrons," Phys. Rev. A **90**, 012706 (2014).
[37]M. D. Epée Epée, J. Z. Mezei, O. Motapon, N. Pop, and I. F. Schneider, "Reactive collisions of very low-energy electrons with H_2^+: Rotational transitions and dissociative recombination," Mon. Not. R. Astron. Soc. **455**, 276–281 (2016).
[38]A. Abdoulanziz, F. Colboc, D. A. Little, Y. Moulane, J. Z. Mezei, E. Roueff, J. Tennyson, I. F. Schneider, and V. Laporta, "Theoretical study of ArH+ dissociative recombination and electron-impact vibrational excitation," Mon. Not. R. Astron. Soc. **479**, 2415–2420 (2018).
[39]J. Z. Mezei, K. Chakrabarti, M. D. Epée Epée, O. Motapon, C. H. Yuen, M. A. Ayouz, N. Douguet, S. F. dos Santos, V. Kokoouline, and I. F. Schneider, "Electron-induced excitation, recombination, and dissociation of molecular ions initiating the formation of complex organic molecules," ACS Earth Space Chem. **3**, 2376 (2019).
[40]D. O. Kashinski, D. Talbi, A. P. Hickman, O. E. Di Nallo, F. Colboc, K. Chakrabarti, I. F. Schneider, and J. Z. Mezei, "A theoretical study of the dissociative recombination of SH^+ with electrons through the $^2\pi$ states of SH," J. Chem. Phy. **146**, 204109 (2017).
[41]M. J. Seaton, "Quantum defect theory," Rep. Prog. Phys. **46**, 167 (1983).
[42]J. Tennyson, "Electron-molecule collision calculations using the *R*-matrix method," Phys. Rep. **491**, 29–76 (2010).
[43]D. A. Little and J. Tennyson, "An ab initio study of singlet and triplet Rydberg states of N_2," J. Phys. B At. Mol. Opt. Phys. **46**, 145102 (2013).
[44]D. A. Little and J. Tennyson, "An R-matrix study of singlet and triplet continuum states of N_2," J. Phys. B At. Mol. Opt. Phys. **47**, 105204 (2014).
[45]H.-J. Werner, P. J. Knowles, G. Knizia, F. R. Manby, and M. Schütz, "Molpro: A general-purpose quantum chemistry program package," WIREs Comput. Mol. Sci. **2**, 242–253 (2012).